Direct Visualization of HIV-1 Replication Intermediates Shows that Capsid and CPSF6 Modulate HIV-1 Intra-nuclear Invasion and Integration

Christopher R. Chin
University of Massachusetts Medical School

Et al.

Let us know how access to this document benefits you.

Repository Citation

Creative Commons License

Direct Visualization of HIV-1 Replication Intermediates Shows that Capsid and CPSF6 Modulate HIV-1 Intra-nuclear Invasion and Integration

Graphical Abstract

Authors

Christopher R. Chin, Jill M. Perreira, George Savidis, ..., Eric M. Feeley, Miles C. Smith, Abraham L. Brass

Correspondence

abraham.brass@umassmed.edu

In Brief

Chin et al. have developed an imaging assay, ViewHIV, which evaluates early HIV-1 replication intermediates. ViewHIV uses available reagents and works with primary cells. Using ViewHIV, they find that CA enters the nucleus and associates with vDNA. Furthermore, CA's interaction with the host factor CPSF6 modulates HIV-1's nuclear entry and integration.

Highlights

- ViewHIV visualizes the HIV-1 capsid and viral DNA in the cytosol and nucleus

- ViewHIV can be done with any HIV-1 strain and primary cells

- ViewHIV shows that CA enters the nucleus and associates with vDNA

- CA's interaction with CPSF6 promotes HIV-1's nuclear entry and integration

CrossMark

CellPress

Direct Visualization of HIV-1 Replication Intermediates Shows that Capsid and CPSF6 Modulate HIV-1 Intra-nuclear Invasion and Integration

Christopher R. Chin,[1,3] Jill M. Perreira,[1,3] George Savidis,[1] Jocelyn M. Portmann,[1] Aaron M. Aker,[1] Eric M. Feeley,[2] Miles C. Smith,[1] and Abraham L. Brass[1,2,4,*]

[1]Department of Microbiology and Physiological Systems, University of Massachusetts Medical School, Worcester, MA 01655, USA
[2]Ragon Institute of Massachusetts General Hospital, MIT and Harvard University, Cambridge, MA 02139, USA
[3]Co-first author
[4]Present address: Department of Microbiology and Physiological Systems, University of Massachusetts Medical School, Worcester, MA 01655, USA
*Correspondence: abraham.brass@umassmed.edu
http://dx.doi.org/10.1016/j.celrep.2015.10.036

SUMMARY

Direct visualization of HIV-1 replication would improve our understanding of the viral life cycle. We adapted established technology and reagents to develop an imaging approach, ViewHIV, which allows evaluation of early HIV-1 replication intermediates, from reverse transcription to integration. These methods permit the simultaneous evaluation of both the capsid protein (CA) and viral DNA genome (vDNA) components of HIV-1 in both the cytosol and nuclei of single cells. ViewHIV is relatively rapid, uses readily available reagents in combination with standard confocal microscopy, and can be done with virtually any HIV-1 strain and permissive cell lines or primary cells. Using ViewHIV, we find that CA enters the nucleus and associates with vDNA in both transformed and primary cells. We also find that CA's interaction with the host polyadenylation factor, CPSF6, enhances nuclear entry and potentiates HIV-1's depth of nuclear invasion, potentially aiding the virus's integration into gene-dense regions.

INTRODUCTION

How HIV-1 overcomes our defenses and infects our cells has been studied intensively for over 30 years. While much has been learned, there remain events in the viral life cycle that resist interrogation. One such area is the initial intra-nuclear portion of infection, from the virus's nuclear entry to its integration into chromatin. We reasoned that an image-based method would be useful for investigating this phase, and so we set about to develop methods that would permit the direct visualization of these early events.

Infection commences with HIV-1's binding to the host receptors, progressing to fusion of the host and viral membranes and entry of the viral core into the cytosol. A conical-shaped assembly comprised of ~250 hexamers and 12 pentamers of capsid protein (CA; Ganser-Pornillos et al., 2007), the core contains two copies of the virus's RNA genome, reverse transcriptase (RT) and integrase (IN). After entry, the core partially uncoats to produce the reverse transcription complex (RTC), wherein RT synthesizes the viral DNA genome (vDNA). HIV-1s with CA mutations have shown that the efficiency of reverse transcription depends on the kinetics of core uncoating (Hulme et al., 2015b; Xu et al., 2013; Yang et al., 2013). The vDNA and its accompanying proteins are referred to as the preintegration complex (PIC). Associating with microtubules, the PIC travels toward the nucleus, gaining access via the nuclear pore complex (NPC). Once within the nucleus, IN interacts with LEDGF, a chromatin-associated factor, resulting in viral integration into actively transcribed genes (Ciuffi et al., 2005). Recent studies have suggested that after 4 days of infection of CD4+ T cells, HIV-1 is found to be predominantly integrated into chromatin located at the nuclear periphery (Marini et al., 2015).

Current models estimate that the final stages of core uncoating occur at the NPC, with the PIC-associated proteins, i.e., CA, being shed prior to nuclear entry (Ambrose and Aiken, 2014; Hilditch and Towers, 2014). While the existence of nuclear PIC-associated CA is under active study, one group's data suggest that CA complexes with nuclear vDNA in primary macrophages, but not in HeLa cells (Peng et al., 2014), while a second work reports CA in HeLa cell nuclei (Hulme et al., 2015a). Several findings argue that CA plays a role in the intra-nuclear viral life cycle (Ambrose et al., 2012; Lee et al., 2010). The polyadenylation factor CPSF6 and the NPC proteins NUP153 and NUP358/RANBP2 interact with CA, thereby influencing nuclear entry and integration sites, although the mechanism is unclear for the latter (Bhattacharya et al., 2014; Matreyek et al., 2013; Price et al., 2012; Schaller et al., 2011). CA mutant viruses that fail to interact with NUP358 or CPSF6 (for example, N74D/A) undergo aberrant integration and, in some instances, exhibit poor fitness (Ambrose et al., 2012; Krishnan et al., 2010; Lee et al., 2010; Schaller et al., 2011).

The majority of these insights were obtained using established molecular virology and biochemistry methods evaluating cell

populations. Importantly, antibody-based imaging of HIV-1 and fluorescence in situ hybridization (FISH) strategies to visualize the viral RNA genome (vRNA) and vDNA (Pezzella et al., 1987; Singer et al., 1989), as well as the use of chimeric viral proteins (Campbell and Hope, 2008; Francis et al., 2014), also have improved our knowledge of HIV-1 infection at a single-cell level. Some of the acknowledged limitations of these approaches are a lack of sensitivity and disruptive preparative conditions (i.e., conventional FISH) and/or an inability to readily distinguish replication-competent viruses from replication-defective viruses (i.e., fluorescent viral fusion proteins). Several methods address such issues, including one employing modified dinucleotide triphosphates (dNTPs) that label reverse-transcribed vDNA (Peng et al., 2014) and another using single-cell imaging of HIV provirus (SCIP, Di Primio et al., 2013), which introduces a restriction enzyme cut site into the vDNA, permitting proviruses to be detected with an exogenous endonuclease.

In a complementary approach, we adapted existing technologies and reagents. Specifically, we use a sensitive branch-chain DNA (bDNA) variant of FISH, ViewRNA (Yang et al., 2006), in combination with immunolabeling using an established anti-CA monoclonal antibody (Simm et al., 1995), to visualize events in early HIV-1 infection in fixed cells. By combining bDNA technology and sandwich hybridization, this approach enhances the detection of nucleic acids (Yang et al., 2006). The ViewRNA probes can be generated to specifically recognize much shorter targets than traditional FISH. This approach also uses a conventional confocal microscope. Among the HIV-1 life cycle events made more appreciable with this approach, we observed that the majority of reverse transcription occurs in the cytosolic periphery of primary macrophages and that loss of the nuclear importer TNP03 prevents PIC nuclear entry via mislocalization of TNP03's cargo, the polyadenylation factor CPSF6. We find that HIV-1 CA enters the nuclei of HeLa cells, U20S cells, and monocyte-derived macrophages (MDMs), and it associates in part with the vDNA, suggesting that CA plays a functional role in HIV-1's intra-nuclear life cycle in both primary and transformed cells. Consistent with this notion, our methods show that either the loss of CPSF6 or point mutations in CA that prevent interaction with CPSF6 decreases nuclear entry as well as the distance that the PIC penetrates into the nucleus, revealing a viral dependency on the host for intra-nuclear trafficking and integration into more centrally located actively transcribed genes.

RESULTS

ViewHIV Identifies Active Viruses by Detecting De Novo Reverse-Transcribed vDNA

In studying influenza A virus genome trafficking, we used an established bDNA-based sandwich hybridization assay, ViewRNA (Yang et al., 2006; Feeley et al., 2011). We estimated that this approach might be useful for studying HIV-1 because (1) it uses a pool of small probes that must anneal in a template-directed manner for signal amplification to occur, (2) the small probes can assemble on less accessible targets, and (3) the probes anneal strand specifically so that they could be designed to preferentially bind to the de novo synthesized vDNA of func-

tional virions rather than the vRNA of inactive particles (Figure 1A). We created four probe sets against the indicated nucleotides of the cDNA of two cloned HIV-1 genomes, NL4-3 and HX2B (Figure 1B); the targeted regions are highly homologous across viral strains. The probe sets are denoted by the viral genes they were designed against as follows: gag, pol (two sets, A and B), and envelope (env).

The env probe set was used in an infection time course (Figure 1C). HeLa-T4 cells were incubated on ice with HIV-IIIB, a CXCR-4-tropic viral population, and then warmed to 37°C to synchronize infection. At the indicated times, the cells were fixed and permeabilized, treated with protease, heated to denature vDNA, hybridized with the env probes, and subsequently confocally imaged. The vDNA was first seen at 4–6 hr post-infection (p.i.), increasing until 12 hr with a decrease at 24 hr. The vDNA signals were seen in the nuclei at 6 hr, with the peak nuclear signal at 12 hr. The mean number of vDNA signals present per nucleus for each condition is provided based on the analysis of ≥10 cells/condition over three experiments. While the exact number of vDNA molecules per signal cannot be determined using this approach, it stands to reason that the magnitude of the signal is proportional to the number of vDNA molecules each one contains; thus, this approach permits a relative, rather than absolute, comparison to be made across samples and experiments. Control samples used heat-killed (HK) virus, an IN inhibitor (entegravir, EVG), or an RT inhibitor (azidothymidine, AZT). The AZT-treated samples had ~20-fold less vDNA signal at 12 hr p.i. than the untreated samples, indicating that the probe preferentially recognized de novo RT products. By 24 hr p.i., when the majority of the HIV-1 has integrated (Butler et al., 2001), the vDNA signal of the HIV-1 alone samples had a ~9-fold decrease in vDNA signals compared to the EVG samples, suggesting that the integration of the vDNA may prevent the probe set's hybridization. In instances of many vDNA signals, there may be overlap so the level detected may be an underestimate. The low level of vDNA in the 24 hr p.i. AZT samples was likely from incomplete RT inhibition. These data demonstrate that the ViewHIV assay preferentially detects the vDNA products of functional viruses carrying out reverse transcription. Because the ViewHIV probe only detects the newly synthesized vDNA, and not the host DNA, this method allows the tracking over time of the vDNA component of the PIC, from its synthesis by RT in the cytosol to its subsequent nuclear entry.

The ViewHIV Assay Reveals that CA Enters the Nuclei of HeLa Cells and Partially Colocalizes with vDNA

As noted, several lines of evidence point toward a nuclear role for CA. Both the level and timing of CA dissociation from the viral genome is a topic of active inquiry, with published data now suggesting that CA enters the nuclei of MDMs and HeLa cells (Hulme et al., 2015a; Peng et al., 2014). In a complementary effort, we visualized CA along with the vDNA using the ViewHIV approach in conjunction with an anti-CA antibody. We tested several antibodies under the ViewHIV conditions with or without the protease treatment step (Figure S1A). Only the AG3.0 monoclonal antibody, which detects p24 from HIV-1, HIV-2, or SIV (Simm et al., 1995), produced a signal with or without protease treatment, with the former condition providing a markedly stronger
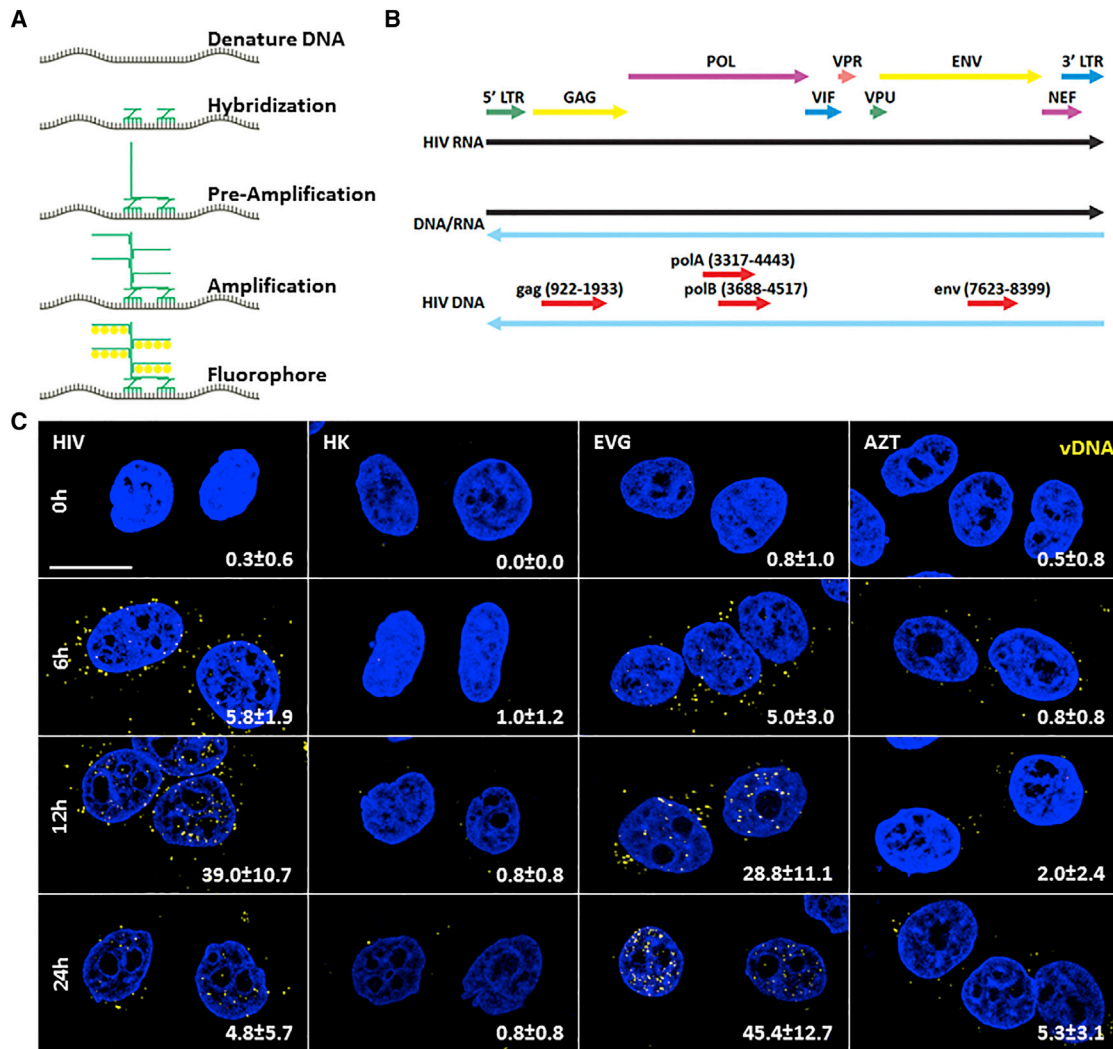
Figure 1. The ViewHIV System Identifies Active Viruses by Detecting the vDNA Product of Reverse Transcription

(A) Schematic model of the ViewRNA assay. After protease treatment and heat denaturation, hybridization probes (green Zs) are annealed to the target vDNA. Pre-amplification probes (green Ls) are used to recognize pairs of hybridization probes that have correctly annealed to adjacent sights. Amplification probes and fluorophores build on this nexus to produce a specific amplified signal.

(B) The ViewHIV probe sets (gag, polA, polB, and env; red arrows, with the base pairs provided) were designed against regions indicated in the HIV-1 vDNA (blue arrow). Additional arrows indicate the HIV-1 genes.

(C) HeLa-T4 cells were infected with either HIV-IIIB (HIV, MOI ~350) or a heat-killed (HK) sample. Either azidothymidine (AZT) or elvitegravir (EVG) was used in matching samples. The cells were then fixed at the indicated times. Samples were processed to detect vDNA (env VF10-10752 probe set, yellow) and host cell DNA (DAPI, blue) and confocally imaged. Quantification of HIV-1 vDNA signals detected in the nucleus (mean ± SD) is provided and was undertaken using image analysis software. Scale bar, 10 μm. Images from three independent experiments, with more than ten cells per experiment, were analyzed for each condition.

result (Figure S1B). The baseline signal (no protease treatment) is consistent with data from publications using the AG3.0 antibody under similar conditions to those here (Fricke et al., 2014; Lukic et al., 2014). In addition, only protease treatment together with AG3.0 showed CA in the nucleus. We conclude that protease treatment enhances a weaker baseline AG3.0 signal (Supplemental Experimental Procedures).

The ViewHIV assay was done in combination with anti-CA AG3.0 immunolabeling in HeLa-T4 cells synchronously infected with HIV-IIIB (Figure 2A). The vDNA and CA were detectable in the cytosol, with 67% ± 8% of vDNA colocalizing with CA in the cytosol at 12 hr p.i. (Figures 2B and 2C). CA signal decreased when an RT inhibitor, nevaripine (NVP), was used, suggesting that the CA epitope recognized by AG3.0 is more accessible upon reverse transcription, potentially via core uncoating. Thus, reverse transcription and proteolysis both enhance CA detection by AG3.0. The approach showed that CA entered the nuclei of HeLa cells by 12 hr p.i., with the majority of intra-nuclear CA co-localizing with vDNA (61% ± 9%, Figures 2B and 2C). These data are inconsistent with that of Peng et al. (2014), but similar to data from another group (Hulme et al., 2015a); such differences may arise from the use of distinct protocols and antibodies. Staining
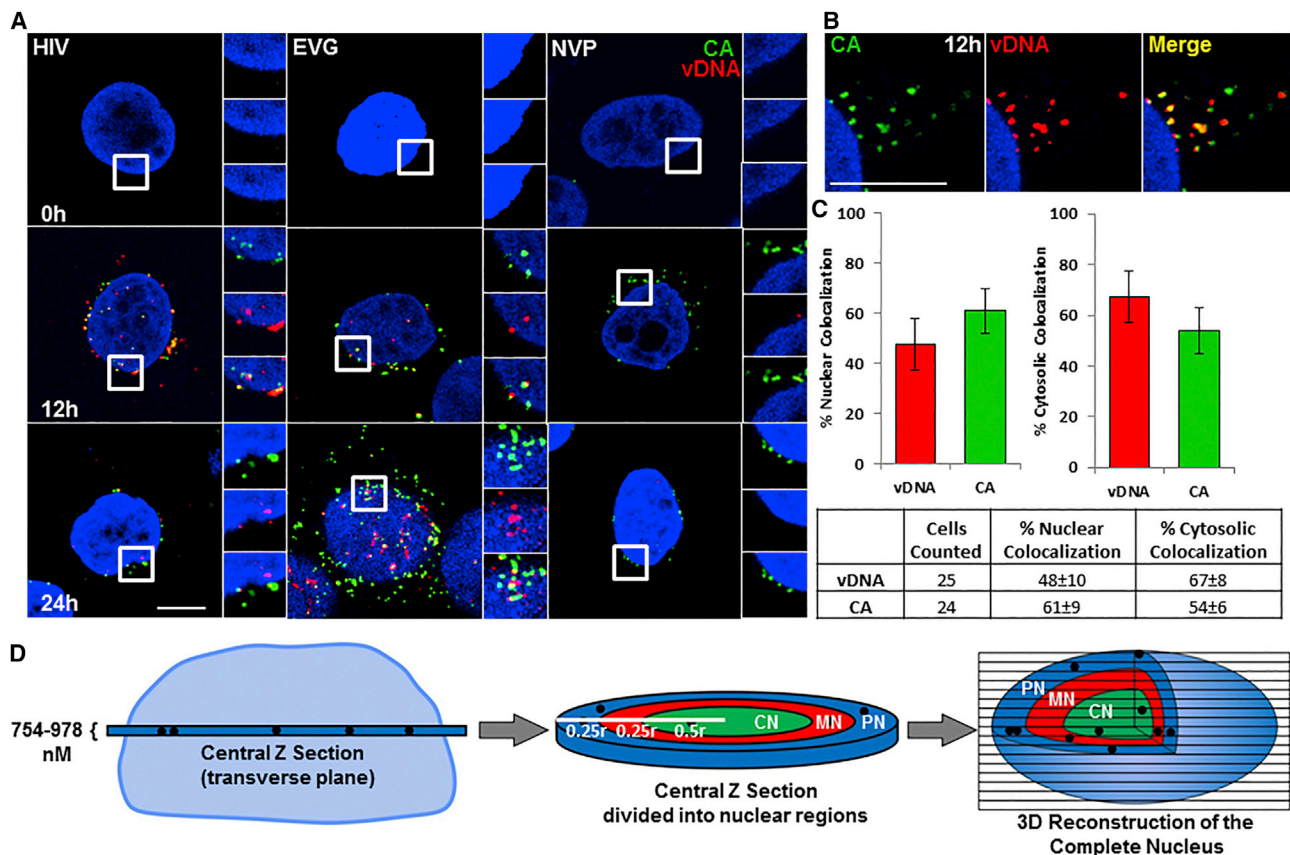
Figure 2. CA Enters the Nuclei of HeLa Cells and Partially Colocalizes with vDNA

(A and B) HeLa-T4 cells were synchronously infected with HIV-IIIB (HIV, MOI ∼350), with or without EVG or nevarapine (NVP), and fixed at the indicated times. Samples were processed to detect vDNA (env VF10-10752 probe set, red), HIV-1 CA (anti-CA AG3.0 antibody, green), and host cell DNA (DAPI, blue) and confocally imaged. Scale bars, 10 μm.

(C) Quantification of HIV-1 vDNA signals colocalizing with CA (or vice versa) in the cytosol or nucleus (mean percentage colocalization ± SD) at 12 hr p.i. as determined using image analysis software. For (A)–(C), images from three independent experiments, with eight or more cells per experiment, were analyzed for each condition.

(D) A schematic cartoon of a representative nucleus (left) and a central z section (center) of 754- to 978-nm thickness. A 3D reconstruction of the entire nucleus (right) was created by assembling all of the z sections that contained portions of the nucleus as determined by DAPI staining of nuclear DNA. To assess the intra-nuclear distribution of viral signals, the central z section and 3D reconstructed nucleus were segmented into three regions as follows: peripheral nuclear (PN, blue), middle nuclear (MN, red), and center nuclear (CN, green) regions, with the fraction of the radius (r) of the nucleus they represent provided.

for the nuclear envelope protein, Lamin B1, revealed no difference in the number of viral signals (HIV-IIIB) assigned to the nucleus using boundaries defined with either Lamin B1 or DAPI (Figure S1C). Therefore, we used the DAPI signal to define nuclear boundaries throughout. We examined the possibility that the CA detected in these assays is not brought in by the incoming virus, but instead represents de novo protein synthesis occurring post-infection. Assays performed with or without the protein translation inhibitor Lactimidomycin (LACT) (Schneider-Poetsch et al., 2010) detected no difference in CA signals (Figure S1D), demonstrating that the CA detected is brought by the incoming virus. These data show that CA enters the nucleus and colocalizes with vDNA in HeLa cells.

Determining the Best Way to Detect the Viral Signals
The Leica SP-5 confocal microscope used for this work captures image sections in the transverse plane (xy plane, parallel to the adherent surface) that are 754–978 nm deep in the z plane, depending on the wavelength of light used (z sections, Figure 2D; Experimental Procedures). For HeLa and U2OS cells, images comprising one complete nucleus consist of 12–17 sequential z sections, with the most centrally located z section in this stack being defined as the central z section. To determine the best method for the detection of viral signals, we compared the number of vDNA or CA signals detected in the central z section with the total number of signals detected in a 3D reconstruction of the corresponding nucleus using all of the DAPI-containing z sections (vDNA, Figures 3A–3F) or in the 3D reconstruction of the entire cell (CA, Figures S2A–S2C), over a wide range of MOIs; this comparison showed a near linear relationship between the respective central z section and 3D reconstruction values. These experiments also showed that serially diluting the viral supernatant led to proportional changes in the viral signals detected, even down to the detection of a single viral signal per nucleus
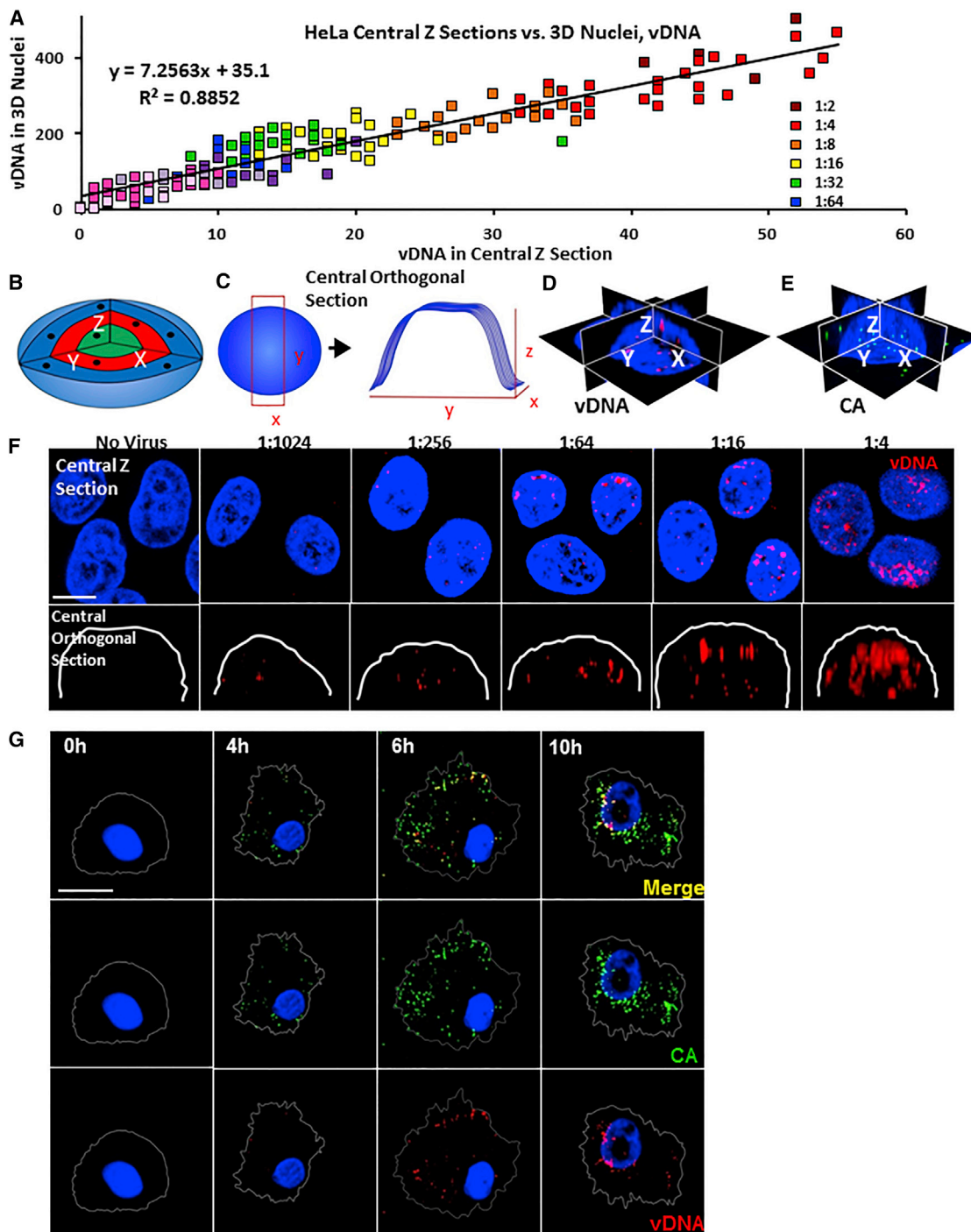
Figure 3. Evaluation and Comparison of Viral Signals Detected with ViewHIV

(A) HeLa-MAGI cells were infected with serial dilutions of HIV-IIIB (MOI ~3–500). Ratios in the legend represent the fold dilution of the viral supernatant (relative MOI). At 24 hr the cells were fixed and processed to detect integrated proviruses (vDNA) using image analysis software from both central z sections (vDNA in central z sections) and 3D reconstructions of the entire corresponding nucleus (vDNA in 3D nuclei). These values were plotted and a linear regression analysis ($R^2 = 0.8852$) was performed.

(B) Schematic of nucleus with color-coded regions (CN, green; MN, red; and PN, blue) and x, y, and z axes. Black dots represent viral signals.

(C) Schematic shows central orthogonal section in map view (left) and elevation view with perspective (right), the latter with the adherent cell surface lying in the xy plane.

(D and E) Schematic shows a central z section (xy plane) and two corresponding central orthogonal sections (zx and zy orthogonal planes) with vDNA (red, D) or CA (green, E) signals.

(legend continued on next page)

or cell. Therefore, the viral signals detected in central z sections permit comparisons over a wide range of MOIs to be made between cells and samples, similar to the results obtained by evaluating complete nuclei or cells.

Using the 3D nuclear reconstructions as a start, we also generated image sections that are orthogonal to the central z section transverse plane and of comparable volumes, referred to as central orthogonal sections (Figures 3B–3E); these would be analogous to coronal plane images in an anatomic setting. This was done to evaluate if CA and vDNA were clearly within the nucleus in both planar surface orientations, as well as to determine in what regions of the nucleus these viral signals were detected. The latter analysis was structured by dividing the nucleus into three regions of equivalent volumes as follows: peripheral nuclear (PN), middle nuclear (MN), and central nuclear (CN, Figure 2D; Experimental Procedures); these studies found that CA and vDNA were detected within the nucleus using both the central z and central orthogonal sections, and with the same relative regional distributions (Figures 3F and S2).

To further test the validity of using the central z section for these analyses, both the number and distribution of viral signals (CA and vDNA) in the central orthogonal section of each nucleus (shown as zy or zx planes, Figure S3A) were compared with these same values obtained by analyzing the central z section (xy plane) of the corresponding nucleus (Figures S3A–S3E); as seen with the 3D reconstruction versus central z section comparisons, both the number and position of the CA and vDNA signals were very similar between the paired central orthogonal and central z sections. Therefore, when viral signals per nucleus are provided in the text or figures, those values represent the signals detected in the central z section.

The ViewHIV Assay Detects CA that Partially Colocalizes with vDNA in the Nuclei of Primary Macrophages

To determine if this approach can detect CA entering the nucleus in cells that are relevant to HIV-1 infection in vivo, we tested the ViewHIV assay on MDMs from patient donors. Using HIV-1 BaL virus, a CCR5-tropic viral population, we initiated a synchronized infection and then processed the cells at the indicated times (Figures 3G and 4A). The vDNA was detected in the untreated and EVG samples, but not in the HK virus or NVP samples. Similar to the data in HeLa cells, vDNA first appeared in the peripheral cytosol of the MDMs at 4–6 hr, with the greatest level of vDNA signals being detected at 12 hr in the untreated samples and at 24 hr in the EVG samples (Figure 4A).

The ViewHIV probe set was used in combination with the anti-CA antibody in assays with MDMs (Figures 3G and 4B). Similar to HeLa cells, CA entered the nuclei of MDMs and colocalized in part with vDNA (Figures 3G, 4B, and 4C). These data are consistent with the results of Peng et al. (2014); 59% ± 10% of the nuclear CA colocalized with vDNA (Figures 4D and S3F). Similar

to the HeLa cells, most of the vDNA and CA signals were lost by 24 hr p.i. The inhibition of integration also increased the level of nuclear vDNA and CA. An RT inhibitor (AZT) resulted in not only less vDNA signal but also less CA signal. We note that although the levels of both CA and vDNA signals were considerably lower in MDMs than in HeLa cells, their presence supports the relevance of results using transformed cells.

Using the ViewHIV Approach to Evaluate the Roles of Host Factors in HIV-1 Replication

We next assessed the usefulness of the ViewHIV approach to investigate the role of host factors (MxB, WNK1, and COG2 and 3) in viral replication (Supplemental Experimental Procedures; Figures S4A–S4H and S5A–S5G). The host factors NUP153, TNPO3, and CPSF6 all modulate HIV-1 nuclear entry and integration (Brass et al., 2008; Christ et al., 2008; Lee et al., 2010). Hypotheses regarding the role of TNPO3 in HIV-1 replication include it being the nuclear importer of HIV-1, as well as it being needed to prevent the accumulation of cytosolic CPSF6, which binds to the PIC and prevents it from entering the nucleus (De Iaco et al., 2013; Hilditch and Towers, 2014). There also has been debate over what stage in viral replication TNPO3 is needed, either before or after HIV-1 nuclear entry (De Iaco et al., 2013).

We depleted CPSF6 alone, or with TNPO3 or NUP153, in HeLa-T4 cells, then infected the cells with HIV-IIIB. We immunostained for CA and CPSF6 and detected vDNA at 12 hr p.i. (Figure 5A; 0- and 12-hr samples immunostained for CSPF6 are provided; Figures S5H and S5I). The relative percentage of nuclear entry was quantified by determining the number of vDNA and CA particles as compared to the non-targeting (NT) controls (Figure 5B). These experiments showed that, consistent with some reports (Christ et al., 2008; De Iaco et al., 2013; Zhang et al., 2010), TNPO3 and NUP153 are required for HIV-1 nuclear entry, with a 5-fold decrease in both vDNA and CA nuclear entry seen with their loss. The levels of vDNA and CA in the nuclei were similar, suggesting they physically associate during, and for some time after, nuclear entry. CPSF6 depletion alone decreased viral nuclear entry at 12 hr p.i. by 1.8-fold. Consistent with some reports, loss of both CPSF6 and TNPO3 resulted in restoration of viral nuclear entry to the levels seen with the loss of CPSF6 alone (Ambrose et al., 2012; De Iaco et al., 2013). In contrast, loss of CPSF6 did not similarly increase nuclear entry when NUP153 was targeted, indicating that the former dynamic is specific to TNPO3. The levels of total (cytosolic and nuclear) CA and vDNA signals were found to be similar (Figure S5J).

Immunoblotting confirmed target depletion (Figures 5C and 5D). Increasing the detector sensitivity revealed more cytosolic CPSF6 in the TNPO3-depleted cells (Figure 5E). Quantitation of the cytosolic colocalization between CPSF6 and CA showed a 10-fold increase in the TNPO3-depleted cells (Figure 5F),

---

(F) Comparison of central z section and central orthogonal section images from (A) with the nuclear periphery in white. Representative images for several MOIs are provided showing proviral (vDNA) signals in a central z section (red) and a matching central orthogonal section from the same nucleus. Ratios above the top panels represent the fold dilution of the viral supernatant used. DNA, blue; vDNA, red. Scale bar, 5 μM.

(G) MDMs were synchronously infected with NL4-3 BaL virus and fixed at the indicated times then processed to detect vDNA (gag VF6-12978 probe set, red), CA (green), or nuclear DNA (blue). Image analysis software was used to create cytosolic outlines (white). Images are representative of those seen in four experiments each using cells from different donors. Scale bar, 10 μM.
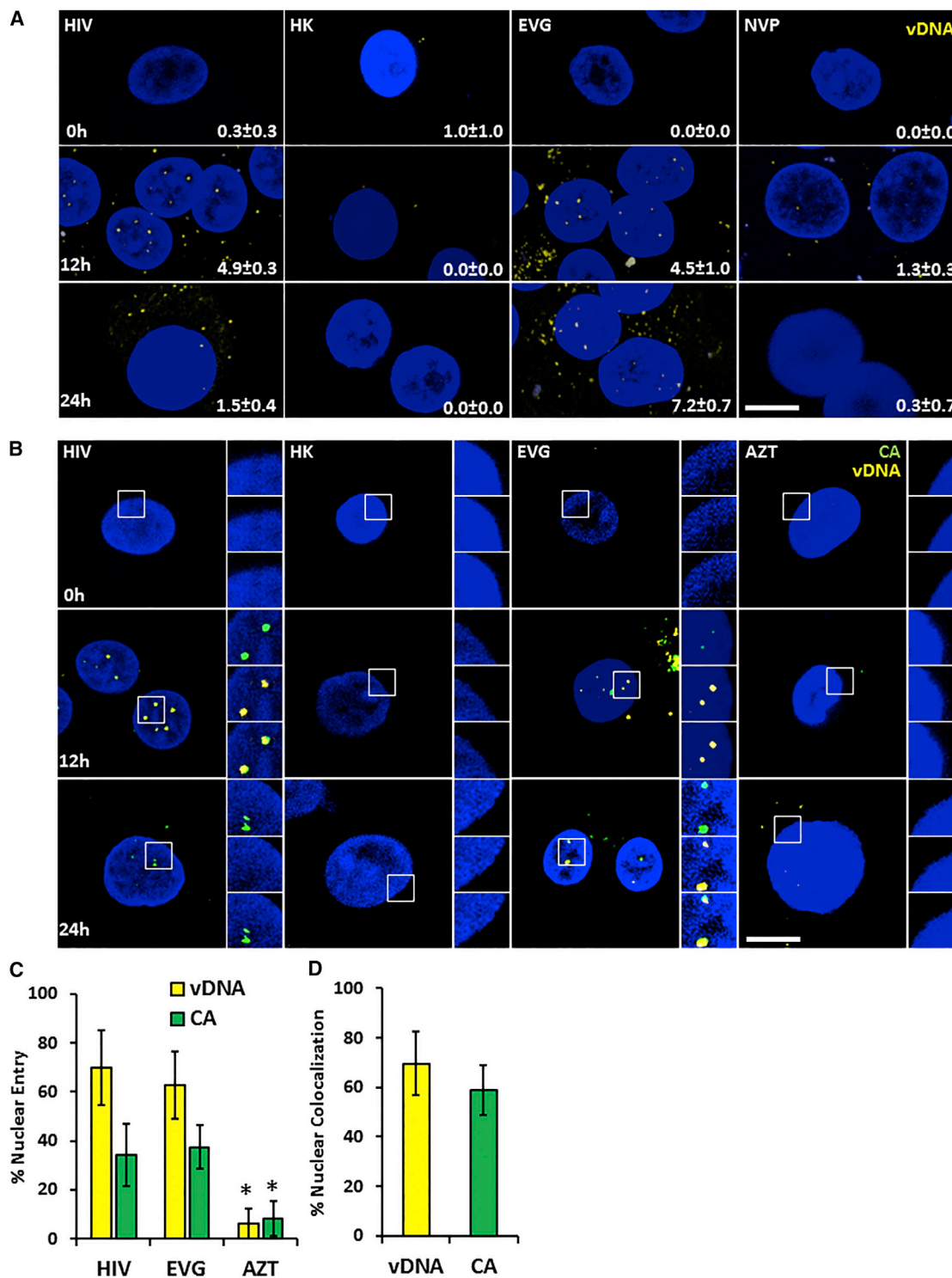
Figure 4. CA Colocalizes with vDNA in the Cytosol and Nuclei of MDMs

(A) MDMs were synchronously infected with HIV-BaL (HIV, MOI ~50), an HK control, or with EVG or NVP and fixed at the indicate times. Samples were processed to detect vDNA (gag VF6-12978 probes, yellow) and host DNA (blue) and confocally imaged. Numbers show the quantification of nuclear vDNA signals (mean ± SD). Scale bar, 10 μm.

(B) As in (A) and samples were processed for vDNA (gag VF6-12978 probe set, yellow), CA (anti-CA AG3.0, green), and host DNA (DAPI, blue) and confocally imaged. Scale bar, 10 μm.

consistent with cytosolic CPSF6 binding to CA and preventing nuclear entry.

A 2-LTR circle assay was performed side by side (Figure 5G). Consistent with the ViewHIV data, there was a 3-fold defect in 2-LTR circles in the absence of TNPO3, and this phenotype was dependent on CPSF6. No loss of 2-LTR circles was seen with CPSF6 depletion, in contrast to the ViewHIV assay data. The 2-LTR circle assay was done at 24 hr p.i., which may allow additional HIV-1 nuclear entry in the absence of CPSF6, as compared to the ViewHIV assay that was done at 12 hr p.i. When viral replication was assessed by CA staining in matched samples after 48 hr, a decrease was seen with TNPO3 depletion and this was dependent on CPSF6 (Figure 5H). In contrast, the dependency of HIV-1 on NUP153 was not affected by CPSF6 levels. In keeping with previous reports, loss of CPSF6 did consistently lower HIV-1 replication at 48 hr p.i., although the effect was modest (Figures 5H and S5K; Ambrose et al., 2012; Schaller et al., 2011). Interestingly, when comparing the results of the two nuclear entry assays (ViewHIV and 2-LTR circle), the ViewHIV assay had greater sensitivity. These data suggest that, in the absence of TNPO3, CPSF6 remains in the cytosol and binds to the CA portion of the PIC, thus preventing viral nuclear entry.

The Polyadenylation Factor CPSF6 Modulates the Depth of HIV-1 Intra-nuclear Invasion and Integration

Given that CA and vDNA associate in nuclei, that CA binds CPSF6, and that loss of CPSF6 decreases HIV-1 nuclear entry, we further investigated how CPSF6 modulates HIV-1 replication. We depleted U20S cells of CPSF6, then infected them with either NL4-3 (wild-type, WT) or an isogenic NL4-3 virus containing an N74A mutation that prevents interaction with CPSF6 (Figure 6A; Matreyek et al., 2013). Both viruses were pseudotyped with VSV-g protein. Equivalent RT units of each virus were used for these experiments and this was done for all such experiments. In cells transfected with the NT small interfering RNA (siRNA), >85% of the N74A CA was located at or near the PN, with only 10% located in the MN, and <1% in the CN (Figures 6A and 6B; see Figure 2D for nuclear region diagram). In contrast, the WT CA was more evenly dispersed throughout the nucleus with 44% of the virus at the PN, 30% of the virus in the MN, and 26% of the virus in the CN. When comparing the WT virus under conditions of normal (NT) or reduced CPSF6 levels, CA was dispersed throughout the nucleus in the NT-transfected cells. When CPSF6 was depleted, the distribution of WT CA changed so that >85% of the CA was confined to the PN, 12% to the MN, and only 1% to the CN (Figures 6A and 6C). These data show a similarity between the effects on CA intra-nuclear migration seen with a virus that does not interact with CPSF6, N74A, or with reduction of CPSF6. These results demonstrate that CPSF6 interacting with CA is required for CA's trafficking within the nucleus.

We next investigated whether the loss of the CA-CPSF6 interaction also modulated the sites of viral integration into the host chromatin. The vDNA signal decreased using the standard ViewHIV protocol at around ≥24 hr p.i. This suggests that detection of the integrated vDNA (proviruses) was prevented by its incorporation into chromatin and that a protocol more similar to the one used for chromosomal FISH might permit proviral detection.

We also wished to compare this approach to the SCIP method for detecting proviruses (Di Primio et al., 2013). U20S cells were transfected with either a negative control siRNA (NT) or an siRNA targeting CPSF6. Then, 24 hr later, the cells were transfected with the plasmid pCBASceI, which expresses the SceI restriction enzyme. At 72 hr post-siRNA transfection, the cells were infected with HIV-1 containing an SceI recognition site, HIV-CMV-delta-GFP-I-SceI WT, which was pseudotyped with VSV-g. Then, 24 hr later the cells were either processed to detect proviruses using a modified ViewHIV protocol (pressurized denaturation step and an expanded probe set that covers the entire NL4-3 genome, Figure 6D; Table S1) or with the SCIP method (Figure 6E). Similar to the CA data, the ViewHIV approach to detect proviruses also revealed a difference between the control cells and the CPSF6-depleted cells, with the latter showing >70% of the proviruses (vDNA) located at or near the PN, and only 22% located in the MN and 0.05% in the CN (Figure 6D). In contrast, the control cells (NT) had proviruses that were more dispersed throughout the nucleus with 35% of the virus located at the PN, 37% of the virus in the MN, and 28% of the virus in the CN. In addition, the total number of proviruses was lower with CPSF6 depletion, consistent with the defect in nuclear entry seen earlier. When we used the SCIP assay, employing the SceI restriction site-containing virus in conjunction with transfected SceI and γ-H2AX immunostaining on the cells from the same experiments as immediately above, we observed a similar result when CPSF6 was reduced, with 68% of the γ-H2AX foci (proviruses, integrated vDNA) detected in the PN, 23% in the MN, and 0.09% in the CN (Figure 6E). We also assessed viral integration after 24 hr using an additional CA mutant virus, A105T (Lee et al., 2010), which like N74A cannot bind to CPSF6 (Figure S6A). Similar to what was seen with CSPF6 depletion, the two mutant viruses that do not interact with CPSF6 produced less integration events at 24 hr p.i. than WT virus; the mutant CA viruses also were found to preferentially integrate at the periphery of the nucleus as compared to the WT proviruses.

To examine the distribution of PICs of the WT and N74A mutant viruses in the same nucleus, we made two lentiviruses differing only in that each contained a distinct non-translatable (no start codon) reporter gene (either GFP or *discoma* species red [DsRed]). We then created VSV-g pseudotyped lentiviruses using these partial HIV-1-genomic reporter plasmids, together with either a standard lentiviral packaging plasmid, pPAX2 (which supplies WT gag and pol in *trans*), or a version of pPAX2 coding for the N74A CA mutation. The WT-DsRed and N74A-GFP viruses were then used singly or in combination to infect U20S cells for 12 hr (Figure S6B). These experiments

---

(C) Quantification of the percentage of the total vDNA or CA signals (nucleus and cytosol) detected in the nucleus (mean ± SD) at 12 hr p.i. is shown.

(D) Quantification of the percentage of the nuclear vDNA signals colocalizing with CA, or of the nuclear CA signals colocalizing with vDNA, in host cell nuclei (mean percentage nuclear colocalization ± SD) at 12 hr p.i. is shown. Images from three experiments each using different donors, with >10 cells per experiment, were analyzed for each condition (*p ≤ 0.05, Student's t test).
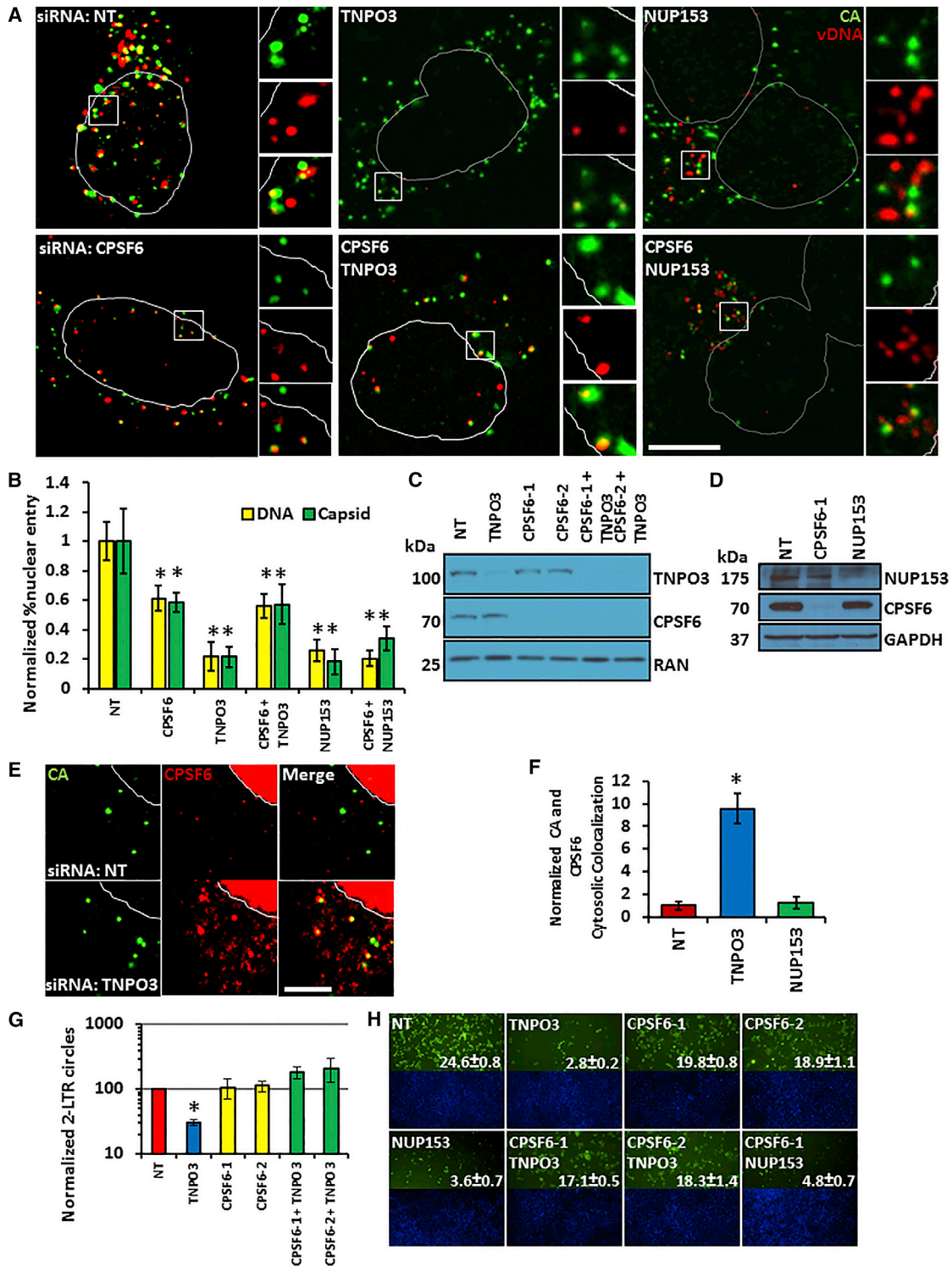
Figure 5. Evaluating the Roles of TNPO3, NUP153, and CPSF6 in HIV-1 Nuclear Entry

(A) HeLa-T4 cells were transfected with the indicated siRNAs. Then, 72 hr later, the cells were synchronously infected with HIV-IIIB (MOI ~300), then fixed at 12 hr p.i. and processed to detect CA (green) and vDNA (gag VF6-12978, red). CPSF6 indicates CPSF6-1 siRNA seen in (B)–(D), (G), and (H). Image analysis software was used to create nuclear outlines based on DAPI staining of host DNA (white). Scale bar, 5 μm.

(B) Image analysis software was used to determine the percentage of the total CA or vDNA (DNA, nucleus and cytosol) signals that were present in the host cell nuclei after transfection with the indicated siRNAs. The values (mean ± SD) have been normalized to those of the NT control.

(legend continued on next page)

revealed differences in PIC nuclear entry and intra-nuclear trafficking between the WT-DsRed and N74A-GFP viruses similar to those above, thereby demonstrating that the ViewHIV technique can be used to recognize distinct viral populations in the same cell.

In an orthologous approach, we used WT CA and N74A CA versions of pPAX2 to package the SceI site-containing viruses. Equivalent RT units of the resulting viruses (WT CA-SceI and N74A CA-SceI) were then used and showed that the differences in both the number and nuclear distribution of WT and N74A proviruses found with the ViewHIV method also were detected using the SCIP method (Figure S6C). CA staining also was readily appreciated at 12 hr p.i. of cells with the WT-DsRed and N74A-GFP, again arguing against these signals arising from the de novo translation of CA post-infection because these viruses do not contain a *gag* gene (Figure S7A).

Comparable differences between the WT virus and the N74A and A105T CA mutant viruses were obtained in studies using either MDMs or CD4+ T cells from multiple donors (Figures 7A, 7B, S7B, and S7C). Central orthogonal sections from the nuclei of infected CD4+ T cells demonstrated similar differences in proviral nuclear prevalence and distribution between the WT NL4-3 virus and the N74A CA mutant virus as those seen using central z sections (Figures 7C and S7D). In keeping with the data generated in HeLa cells, a near linear relationship was detected when comparing the number of vDNA signals in the central z sections to those found in matched 3D nuclear reconstructions, further validating that the analysis of the central z section represents what is occurring in the nucleus as a whole (Figure S7E). These data reveal that the CA-CPSF6 interaction governs (1) the level of viral nuclear entry, (2) the depth the PIC invades into the nucleus, and (3) how deeply within the nucleus viral integration occurs. In light of published data showing that the N74D CA mutant viruses integrated into less actively expressed genes than WT viruses (Schaller et al., 2011) and the known predilection of the polyadenylation factor CPSF6 for sites of ongoing transcription, these data also support a role for intranuclear CA-CPSF6 interactions facilitating HIV-1's preference for integration into actively transcribed genes (Figure 7D).

DISCUSSION

This work describes an image-based approach, ViewHIV, that visualizes the early events of HIV-1 infection, from reverse transcription to viral integration. Some advantages of this approach are its use of commercially available probe sets designed against conserved regions of the HIV-1 genome, allowing for the majority of HIV-1 variants to be studied, including clinical isolates. By targeting the negative strand of the vDNA, the ViewHIV probes preferentially detect active viruses capable of undergoing reverse transcription and separate functional particles from the greater majority of ineffective viruses. The ViewHIV signals arise from the assembly of smaller probes, permitting evaluation of less accessible areas (i.e., the nucleus). Similar results were obtained for CA and cytosolic vDNA detection using antibodies and exogenous modified nucleotides (Peng et al., 2014); like the ViewHIV assay, this method also allows the identification of active viruses. However, in contrast to our approach, the method of Peng et al. (2014) non-specifically labels all DNA being synthesized within the cell, including the host's DNA, thus making it difficult to follow vDNA nuclear entry. The ViewHIV method also uniquely permits the monitoring of different viruses within the same cell using virus-specific probes.

The ViewHIV approach also visualizes integrated vDNA (proviruses), a stage of the viral life cycle detected by the SCIP method (Di Primio et al., 2013). A side-by-side comparison of the two approaches in this study showed similar results and efficiencies. A weakness of the proviral ViewHIV approach is that it does at times detect a low level of signal near to the nucleus; this could result from the recognition of some remaining unintegrated vDNA or from the pressurized denaturation step extruding some chromatin. The SCIP protocol can be done without protease and heating steps and does not recognize unintegrated vDNA. The ViewHIV approach can be done using clinical isolates and without the exogenous expression of a restriction enzyme; it also does not rely on the production of double-stranded DNA (dsDNA) breaks, which produce background.

The ViewHIV approach detected reverse transcription in the cytosolic periphery of HeLa cells and MDMs starting at about 4 hr p.i., and it confirmed published data showing that CA entered the nucleus of MDMs along with vDNA (Peng et al., 2014). However, in contrast to what was reported by Peng et al. (2014), we also observed CA entering the nuclei of HeLa cells, as well as U20S cells, and this nuclear CA associated with vDNA in many instances. Hulme et al. (2015a) also have reported CA in the nucleus of HIV-1-infected HeLa cells. We are unsure as to why these differences occurred, but one reason may be that the three studies used different anti-CA antibodies. Indeed, we see a large increase in CA signal in the setting of active reverse transcription and with the use of protease, suggesting that epitope accessibility influences the detection of CA by the AG3.0 antibody (Supplemental Experimental Procedures). We note that blocking integration stabilized CA signal in the nucleus at 24 hr p.i., suggesting that integration results in

---

(C and D) Immunoblots of lysates from (A) and (B) using the indicated siRNAs. CPSF6-1 and -2 indicate two distinct siRNAs.

(E) HeLa-T4 cells transfected with non-targeting siRNA (NT) or siRNAs against TNPO3 were immunostained for CA (AG3.0, green) and CPSF6 (red) and imaged using a uniformly higher detector sensitivity than in (A). Scale bar, 2 μm.

(F) Image analysis software was used to determine the level of colocalization between CA and CPSF6 in the cytosol of cells in (E). Values were normalized to the NT control.

(G) A 2-LTR circle assay was performed using lysates from cells transfected with the indicated siRNAs. Values were normalized to the NT control and represent the mean ± SD.

(H) HeLa-T4 cells were transfected with the indicated siRNAs for 72 hr, then infected with HIV-IIIB. Then, 48 hr later, cells were stained for CA (mab183 antibody, green) or host cell nuclei (DAPI, blue). Numbers represent the mean percentage infection ± SD (n = 3, magnification = 4×). For the above data, images from three experiments, with more than ten cells per experiment, were analyzed for each condition (*p ≤ 0.05, Student's t test).
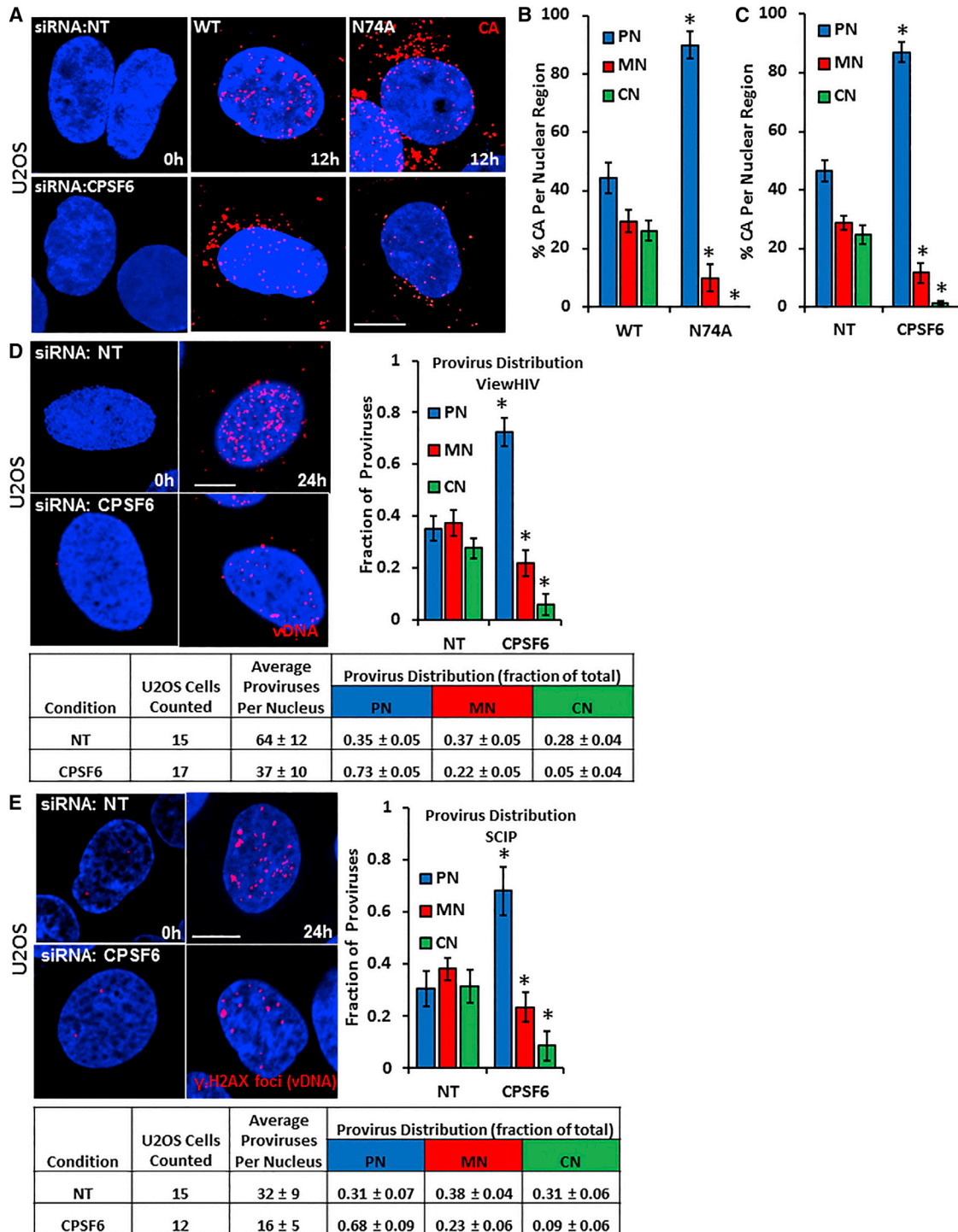
Figure 6. CPSF6 Modulates the Depth of HIV-1 Intra-nuclear Invasion and Integration

(A) U2OS cells were transfected with either NT siRNA or siRNA targeting CPSF6 for 72 hr, then synchronously infected with equivalent RT units of either WT NL4-3 HIV-1 (MOI ~300) or a virus with a point mutation in the CA gene (N74A) that prevents interaction with CPSF6. Cells were fixed 12 hr p.i. and stained for CA (AG3.0 antibody, red) and nuclear DNA (blue). Scale bar, 5 μM.

(B and C) Image analysis software was used to determine the percentage of the total CA detected in each region of the nuclear regions (central z section, PN, MN, or CN). For the WT versus N74A comparison graph (B), the values are from cells transfected with NT siRNA. Numbers represent the mean percentage ± SD.

(D) U2OS cells were transfected with either a negative control (NT) or an anti-CPSF6 siRNA. Then, 24 hr later, the cells were transfected with an expression vector containing SceI; 72 hr post-siRNA transfection, the cells were infected with an HIV-1 virus containing an SceI recognition site, HIV-CMV-delta-GFP-I-SceI,

(legend continued on next page)

CA dissociation. Together these data demonstrate that the genetic determinant of integration, CA (Krishnan et al., 2010; Lee et al., 2010), enters the nucleus and may, therefore, act as a physical determinant of HIV-1 migration and integration.

The ViewHIV approach also was useful in evaluating the roles of TNPO3 and CPSF6 in HIV-1 replication. These data are consistent with the depletion of TNPO3 resulting in excess cytosolic CPSF6, which in turns binds to and retains HIV-1 in the cytosol, thus inhibiting viral nuclear entry; this confirms and expands upon published work (De Iaco et al., 2013; Figure 7D). If CPSF6 is a conditional restriction factor that only acts under settings of low TNPO3, why then does such an ineluctable affinity exist between CA and CPSF6? Our data suggest that viral fitness may depend on the CA-CPSF6 interaction because it governs PIC nuclear entry as well as the distance traveled into the nucleus prior to integration. Results supporting this were obtained using both CPSF6 depletion and mutant viruses that fail to interact with CPSF6. Given the CA-CPSF6 interaction (Henning et al., 2014; Lee et al., 2010; Price et al., 2012) and CPSF6's role in polyadenylation, we favor a model of HIV-1 nuclear entry (Figure 7D) in which the PIC, via CA, interacts with the NPC (NUP358 and NUP153). CPSF6 then binds CA as it moves through the NPC, in conjunction with TNPO3; this ternary interaction serves to disengage the PIC from the NPC and move it into the nuclear periphery. TNPO3 then releases the CSPF6-PIC complex in the nuclear periphery and returns to the cytosol. The PIC is subsequently trafficked through the nucleus via its interaction with CPSF6 to an actively transcribed gene producing RNAs requiring polyadenylation; the remaining CA then dissociates and interactions between IN and LEDGF mediate integration. This is in keeping with the role of CPSF6 in polyadenylation and HIV-1's preferential integration into actively transcribed genes (Craigie and Bushman, 2012). Additional support for this model comes from the lower levels of integration into actively transcribed genes seen with N74D viruses (Schaller et al., 2011). Decreased integration into actively transcribed genes also occurs with depletion of NUP358 or NUP153, both of which interact with CA, suggesting the loss of their docking surfaces may decrease the likelihood that the inbound CPSF6-TNPO3 complex will correctly interact with the PIC and convey it into the nucleus.

In this model (Figure 7D), TNPO3 is critical for preventing CPSF6 from accumulating in the cytosol and instead shuttles CPSF6 to the NPC-bound PIC, where it can bind to CA and enhance HIV-1 nuclear entry. Because PIC nuclear entry is equivalently lowered when either CPSF6 or both CPSF6 and TNP03 are depleted, it suggests that HIV-1 can still more weakly enter the nucleus in the absence of these factors, potentially via CA's interactions with the NPC alone. An additional nuclear importer may be involved, but such an interaction in this model would be predicted to be modulated downstream by CPSF6-CA interactions. This is consistent with the N74A/D and A105T CA-expressing viruses entering the nucleus, albeit at reduced levels, when compared to WT virus. While there have been competing theories as to the role of CPSF6 in HIV-1 infection, our data together with those of others suggest that CPSF6 functions as an HIV-1 dependency factor required for PIC nuclear entry, intra-nuclear migration, and integration (Supplemental Discussion). In conclusion, we envisage the ViewHIV approach to continue being useful for investigating the early stages of the viral life cycle and determining the actions of host factors and small molecules in HIV-1 replication.

EXPERIMENTAL PROCEDURES

HIV Infections

For synchronized infections, all cells were plated on coverslips precoated with sterile rat tail collagen (BD Biosciences) in 24-well plates (Costar). For synchronized infections, cells and virus were pre-chilled on ice for 45 min before the media were aspirated and the viral stocks added to the cells. HK virus was heated at 85°C for 15 min prior to being cooled on ice. The pre-chilled cells were incubated with the cold virus at 4°C for 45 min before being placed at 37°C at time 0. At each time point, cells were washed twice with D-PBS (Life Technologies) and put in 0.025% trypsin (Invitrogen) for 30 s. Cold DMEM (Sigma D5671) containing 10% fetal bovine serum (FBS, Invitrogen 26140079) was used to neutralize the trypsin and wash the cells twice before the cells were fixed for 10 min in 4% formalin (Sigma) in D-PBS. For MDM infections, the cells were pre-treated with dNTPs in complete media for 1 hr prior to infection. The dNTPs (Sigma: dA- D8668, dT- T1895, dC- D0776, and dG- D7145) were kept at a stock of 50 mM (each at 50 mM) and used at 1:500. For CD4+ T cell experiments, cells were chilled on ice for 30 min, mixed with chilled viral supernatants on ice for 40 min, and then placed at 37°C and 5% CO_2 for 4 hr. The cells and viral supernatant were then spun at 1,500 rpm for 10 min and the viral supernatant aspirated, after which the cells were resuspended in complete T cell media with IL-2 and 6-Phosphonohexanoic acid (PHA, see below) and placed back in the tissue culture incubator for a total of 24 hr of infection. At the end of the 24-hr-infection period, the cells were spun as above, the media removed, the cells were fixed for 10 min in D-PBS with paraformaldehyde (PFA 4%, Sigma), and then washed and resuspended with D-PBS.

Cell Culture

For confocal imaging (ViewHIV and immunostaining), HeLa-T4+ cells overexpressing CD4 (NIH AIDS Reagent Repository 154) were plated on glass coverslips in 24-well plates 24 hr prior to infection or transfection. HeLa cells were grown in DMEM with 10% FBS and L-glutamine (Invitrogen 25030081). MDMs and CD4+ T cells were from anonymous human donors per an existing institutional review board (IRB) protocol. Each MDM and CD4+ T cell experiment was performed using a unique donor's cells. MDMs and CD4+ T cells were purified using published methods (Zhu et al., 2014). Base media for culturing the MDMs and CD4+ T cells were RPMI-1640 (Sigma R0883) with 10% FBS (Invitrogen 26140079) supplemented with Non-Essential Amino Acids (Invitrogen 11140-076) and Sodium Pyruvate (Invitrogen 11360-070).

---

pseudotyped with VSV-g (MOI ~400). The cells were fixed 24 hr p.i. and subjected to a modified ViewHIV protocol with increased heat and pressure together with an expanded probe set (HIV NL4-3 Probe Set VF1-14734) designed to recognize integrated proviral DNA (vDNA, red). Cells also were stained with DAPI to detect nuclear DNA (blue). Image analysis software was used to determine the percentage of the total integrated vDNA detected in each region of the nucleus (central z section, PN, MN, or CN). Numbers represent the mean ± SD. Scale bar, 5 μM.

(E) Cells transfected and infected side by side with those in (D) were fixed at 24 hr p.i. and processed using the SCIP assay to detect γ-H2AX foci (integrated vDNA). Image analysis software was used to determine the percentage of γ-H2AX foci (vDNA) detected in each region of the nucleus. Numbers represent the mean ± SD. Scale bar, 5 μM. For the above data, numbers represent the mean ± SD of values derived from three experiments wherein more than ten cells per experimental condition were assessed(*$p \leq 0.05$, Student's t test).
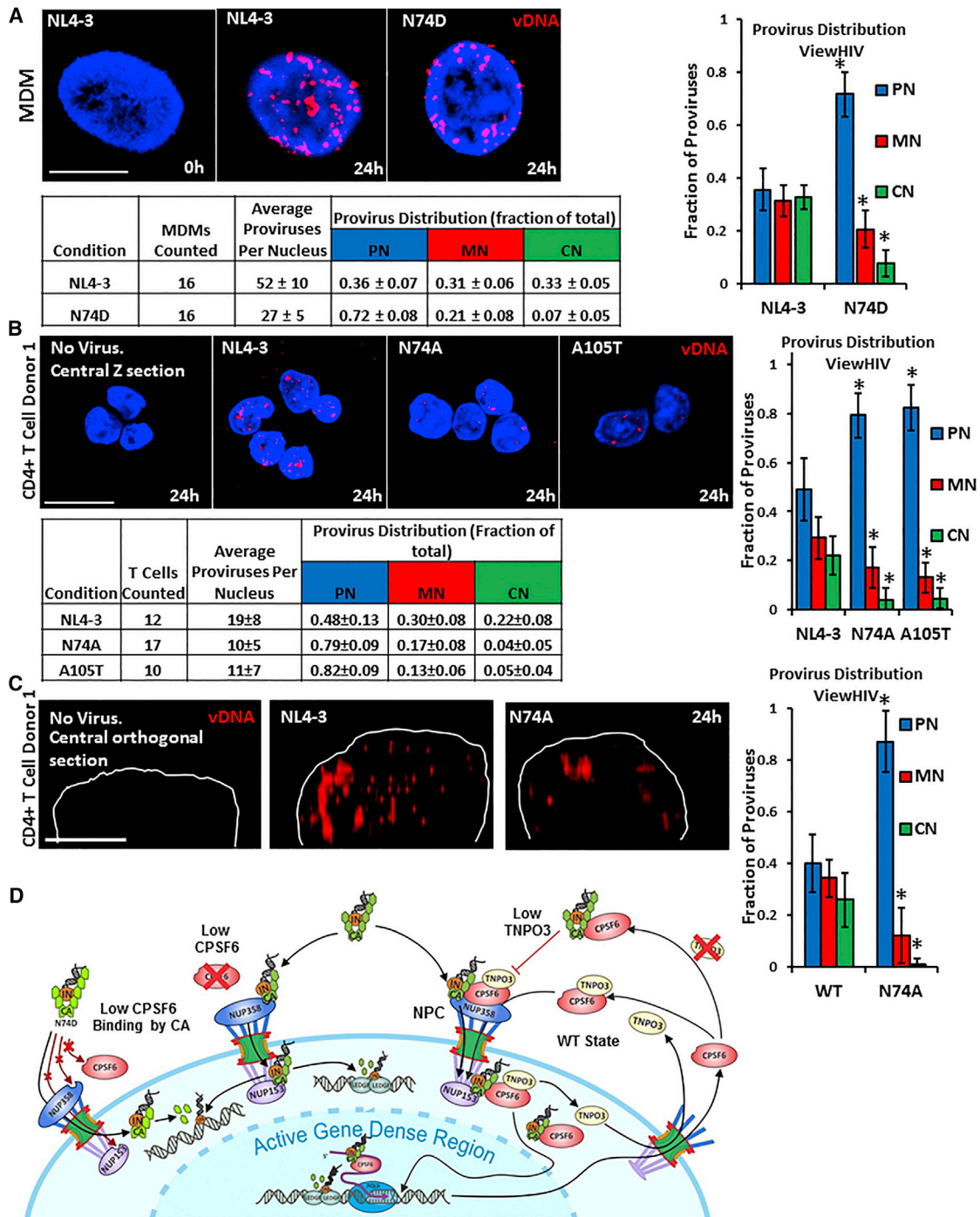
Figure 7. HIV-1 CA Mutant Viruses that Do Not Interact with CPSF6 Show Reduced Nuclear Entry and Intra-nuclear Trafficking in Primary Immune Cells

(A) MDMs were synchronously infected with equivalent RT units of either WT NL4-3 (NL4-3, MOI ∼400) or an N74D mutant virus. The cells were fixed 24 hr p.i. and then subjected to a modified ViewHIV protocol to recognize integrated DNA (vDNA, red). Cells were stained with DAPI to detect nuclear DNA (blue). Scale bar, 10 μM. Image analysis software was used to determine the percentage of the proviral DNA (vDNA) detected in each region of the nucleus (central z section, PN, MN, or CN). Numbers represent the mean ± SD of values derived from three experiments with ten or more cells per condition assessed.

(B) Primary CD4+ T cells were stimulated with PHA then synchronously infected with equivalent RT units of either WT NL4-3 HIV-1 (NL4-3, MOI ∼150) or CA mutant viruses (N74A, A105T). The T cells were fixed 24 hr p.i. and subjected to a modified ViewHIV protocol to recognize integrated vDNA (red). Cells also were stained with DAPI to delimit the nucleus (blue). Scale bar, 10 μM. Image analysis software was used to determine the percentage of the integrated proviral DNA

(legend continued on next page)

MDMs were differentiated in GMCSF (Roche) after plating on glass coverslips in 24-well plates. CD4+ T cells were cultured with IL-2 (50 units/ml, Roche) and PHA-M (5 μg/ml, Sigma L8902).

U20S cells (ATCC) were stably transduced with the Tet-On 3G activator (Clontech Laboratories). The U20S-T3G cells were then stably transduced with a Tet-inducible full-length MxB cDNA.

Viruses

HIV-IIIB and HIV-BaL were from NIH AIDS Reagent Repository. HIV-1 WT NL4-3 and N74A, N74D, and A105T versions were kind gifts of Jeremy Luban (University of Massachusetts Medical School) and Felipe Diaz-Griffero (Albert Einstein Medical School). Pseudotyped viruses were created using the pMD2.G plasmid (VSV-g expressing, Addgene).

The pSCE-1 site containing viral plasmid (HIV-CMV-deltaGFP-I-SceI, SCIP method) and its use in transfections to produce infectious virus has been described previously (Di Primio et al., 2013). The HIV-1 N74A CA mutant version of HIV-CMV-deltaGFP-I-SceI, HIV-CMV-deltaGFP-I-SceI-N74A, was constructed by cloning in a synthesized DNA molecule carrying the corresponding mutation; the resultant construct, pSCE-1-N74A, was then sequence confirmed.

The lentiviral constructs pcVPX-AcGFP-X and pcVPX-dsRed-mono-X were chosen for imaging studies with distinct sets of ViewHIV probes targeting either the reverse transcript of AcGFP (Clontech Laboratories, 632426) or dsRed-monomer-N1 (Clontech Laboratories, 632465) coding sequences (see probe section for details). These fluorophores are divergent in sequence allowing for their simultaneous detection by their corresponding ViewHIV specific probe sets in the absence of appreciable cross-reactivity.

SUPPLEMENTAL INFORMATION

Supplemental Information includes Supplemental Experimental Procedures, seven figures, and one table and can be found with this article online at http://dx.doi.org/10.1016/j.celrep.2015.10.036.

AUTHOR CONTRIBUTIONS

C.R.C., J.M. Perreira, G.S., J.M. Portmann, A.M.A., E.M.F., M.C.S., and A.L.B. performed experiments and wrote the paper.

REFERENCES

Ambrose, Z., and Aiken, C. (2014). HIV-1 uncoating: connection to nuclear entry and regulation by host proteins. Virology 454-455, 371–379.

Ambrose, Z., Lee, K., Ndjomou, J., Xu, H., Oztop, I., Matous, J., Takemura, T., Unutmaz, D., Engelman, A., Hughes, S.H., and KewalRamani, V.N. (2012). Human immunodeficiency virus type 1 capsid mutation N74D alters cyclophilin A dependence and impairs macrophage infection. J. Virol. 86, 4708–4714.

Bhattacharya, A., Alam, S.L., Fricke, T., Zadrozny, K., Sedzicki, J., Taylor, A.B., Demeler, B., Pornillos, O., Ganser-Pornillos, B.K., Diaz-Griffero, F., et al. (2014). Structural basis of HIV-1 capsid recognition by PF74 and CPSF6. Proc. Natl. Acad. Sci. USA 111, 18625–18630.

Brass, A.L., Dykxhoorn, D.M., Benita, Y., Yan, N., Engelman, A., Xavier, R.J., Lieberman, J., and Elledge, S.J. (2008). Identification of host proteins required for HIV infection through a functional genomic screen. Science 319, 921–926.

Butler, S.L., Hansen, M.S., and Bushman, F.D. (2001). A quantitative assay for HIV DNA integration in vivo. Nat. Med. 7, 631–634.

Campbell, E.M., and Hope, T.J. (2008). Live cell imaging of the HIV-1 life cycle. Trends Microbiol. 16, 580–587.

Christ, F., Thys, W., De Rijck, J., Gijsbers, R., Albanese, A., Arosio, D., Emiliani, S., Rain, J.C., Benarous, R., Cereseto, A., and Debyser, Z. (2008). Transportin-SR2 imports HIV into the nucleus. Curr. Biol. 18, 1192–1202.

Ciuffi, A., Llano, M., Poeschla, E., Hoffmann, C., Leipzig, J., Shinn, P., Ecker, J.R., and Bushman, F. (2005). A role for LEDGF/p75 in targeting HIV DNA integration. Nat. Med. 11, 1287–1289.

Craigie, R., and Bushman, F.D. (2012). HIV DNA integration. Cold Spring Harb. Perspect. Med. 2, a006890.

De Iaco, A., Santoni, F., Vannier, A., Guipponi, M., Antonarakis, S., and Luban, J. (2013). TNPO3 protects HIV-1 replication from CPSF6-mediated capsid stabilization in the host cell cytoplasm. Retrovirology 10, 20.

Di Primio, C., Quercioli, V., Allouch, A., Gijsbers, R., Christ, F., Debyser, Z., Arosio, D., and Cereseto, A. (2013). Single-cell imaging of HIV-1 provirus (SCIP). Proc. Natl. Acad. Sci. USA 110, 5636–5641.

Feeley, E.M., Sims, J.S., John, S.P., Chin, C.R., Pertel, T., Chen, L.M., Gaiha, G.D., Ryan, B.J., Donis, R.O., Elledge, S.J., and Brass, A.L. (2011). IFITM3 inhibits influenza A virus infection by preventing cytosolic entry. PLoS Pathog. 7, e1002337.

Francis, A.C., Di Primio, C., Quercioli, V., Valentini, P., Boll, A., Girelli, G., Demichelis, F., Arosio, D., and Cereseto, A. (2014). Second generation imaging of nuclear/cytoplasmic HIV-1 complexes. AIDS Res. Hum. Retroviruses 30, 717–726.

Fricke, T., White, T.E., Schulte, B., de Souza Aranha Vieira, D.A., Dharan, A., Campbell, E.M., Brandariz-Nuñez, A., and Diaz-Griffero, F. (2014). MxB binds to the HIV-1 core and prevents the uncoating process of HIV-1. Retrovirology 11, 68.

Ganser-Pornillos, B.K., Cheng, A., and Yeager, M. (2007). Structure of full-length HIV-1 CA: a model for the mature capsid lattice. Cell 131, 70–79.

Henning, M.S., Dubose, B.N., Burse, M.J., Aiken, C., and Yamashita, M. (2014). In vivo functions of CPSF6 for HIV-1 as revealed by HIV-1 capsid evolution in HLA-B27-positive subjects. PLoS Pathog. 10, e1003868.

(vDNA) detected in each region of the nucleus for the indicated viruses. Numbers represent the mean ± SD of values derived from three experiments with ten or more cells per condition assessed.
(C) Central orthogonal sections from nuclei from cells in (B). Image analysis software was used to determine the percentage of the integrated proviral DNA (vDNA) detected in each orthogonal section for each of more than ten cells for all conditions tested (Figure S7D) (*p ≤ 0.05, Student's t test).
(D) Model of HIV-1 nuclear entry and intra-nuclear trafficking. WT state: the PIC's CA interacts with the NPC, first NUP358/RANBP2 followed by NUP153. As CPSF6 is transported through the NPC by TNPO3, it interacts with CA and disengages the PIC from the NPC. TNPO3 releases the CPSF6-PIC complex and returns to the cytosol. The PIC is ferried through the nucleus by a direct interaction between CA and CPSF6, ultimately arriving at an actively transcribed gene where the interactions between IN and LEDGF mediate integration. Low TNPO3 states increase cytosolic CPSF6, which in turn binds to and retains the PIC in the cytosol preventing nuclear entry. Low CSPF6: PIC nuclear entry and intra-nuclear trafficking are reduced when CPSF6 is depleted or with infection by mutant viruses (N74A/D, A105T) that do not bind CPSF6 (low CPSF6 binding by CA), potentially leading to integration into less transcriptionally active genes.

Hilditch, L., and Towers, G.J. (2014). A model for cofactor use during HIV-1 reverse transcription and nuclear entry. Curr. Opin. Virol. *4*, 32–36.

Hulme, A.E., Kelley, Z., Foley, D., and Hope, T.J. (2015a). Complementary Assays Reveal a Low Level of CA Associated with Viral Complexes in the Nuclei of HIV-1-Infected Cells. J. Virol. *89*, 5350–5361.

Hulme, A.E., Kelley, Z., Okocha, E.A., and Hope, T.J. (2015b). Identification of capsid mutations that alter the rate of HIV-1 uncoating in infected cells. J. Virol. *89*, 643–651.

Krishnan, L., Matreyek, K.A., Oztop, I., Lee, K., Tipper, C.H., Li, X., Dar, M.J., Kewalramani, V.N., and Engelman, A. (2010). The requirement for cellular transportin 3 (TNPO3 or TRN-SR2) during infection maps to human immunodeficiency virus type 1 capsid and not integrase. J. Virol. *84*, 397–406.

Lee, K., Ambrose, Z., Martin, T.D., Oztop, I., Mulky, A., Julias, J.G., Vandegraaff, N., Baumann, J.G., Wang, R., Yuen, W., et al. (2010). Flexible use of nuclear import pathways by HIV-1. Cell Host Microbe *7*, 221–233.

Lukic, Z., Dharan, A., Fricke, T., Diaz-Griffero, F., and Campbell, E.M. (2014). HIV-1 uncoating is facilitated by dynein and kinesin 1. J. Virol. *88*, 13613–13625.

Marini, B., Kertesz-Farkas, A., Ali, H., Lucic, B., Lisek, K., Manganaro, L., Pongor, S., Luzzati, R., Recchia, A., Mavilio, F., et al. (2015). Nuclear architecture dictates HIV-1 integration site selection. Nature *521*, 227–231.

Matreyek, K.A., Yücel, S.S., Li, X., and Engelman, A. (2013). Nucleoporin NUP153 phenylalanine-glycine motifs engage a common binding pocket within the HIV-1 capsid protein to mediate lentiviral infectivity. PLoS Pathog. *9*, e1003693.

Peng, K., Muranyi, W., Glass, B., Laketa, V., Yant, S.R., Tsai, L., Cihlar, T., Müller, B., and Kräusslich, H.G. (2014). Quantitative microscopy of functional HIV post-entry complexes reveals association of replication with the viral capsid. eLife *3*, e04114.

Pezzella, M., Pezzella, F., Galli, C., Macchi, B., Verani, P., Sorice, F., and Baroni, C.D. (1987). In situ hybridization of human immunodeficiency virus (HTLV-III) in cryostat sections of lymph nodes of lymphadenopathy syndrome patients. J. Med. Virol. *22*, 135–142.

Price, A.J., Fletcher, A.J., Schaller, T., Elliott, T., Lee, K., KewalRamani, V.N., Chin, J.W., Towers, G.J., and James, L.C. (2012). CPSF6 defines a conserved capsid interface that modulates HIV-1 replication. PLoS Pathog. *8*, e1002896.

Schaller, T., Ocwieja, K.E., Rasaiyaah, J., Price, A.J., Brady, T.L., Roth, S.L., Hué, S., Fletcher, A.J., Lee, K., KewalRamani, V.N., et al. (2011). HIV-1 capsid-cyclophilin interactions determine nuclear import pathway, integration targeting and replication efficiency. PLoS Pathog. *7*, e1002439.

Schneider-Poetsch, T., Ju, J., Eyler, D.E., Dang, Y., Bhat, S., Merrick, W.C., Green, R., Shen, B., and Liu, J.O. (2010). Inhibition of eukaryotic translation elongation by cycloheximide and lactimidomycin. Nat. Chem. Biol. *6*, 209–217.

Simm, M., Shahabuddin, M., Chao, W., Allan, J.S., and Volsky, D.J. (1995). Aberrant Gag protein composition of a human immunodeficiency virus type 1 vif mutant produced in primary lymphocytes. J. Virol. *69*, 4582–4586.

Singer, R.H., Byron, K.S., Lawrence, J.B., and Sullivan, J.L. (1989). Detection of HIV-1-infected cells from patients using nonisotopic in situ hybridization. Blood *74*, 2295–2301.

Xu, H., Franks, T., Gibson, G., Huber, K., Rahm, N., Strambio De Castillia, C., Luban, J., Aiken, C., Watkins, S., Sluis-Cremer, N., and Ambrose, Z. (2013). Evidence for biphasic uncoating during HIV-1 infection from a novel imaging assay. Retrovirology *10*, 70.

Yang, W., Maqsodi, B., Ma, Y., Bui, S., Crawford, K.L., McMaster, G.K., Witney, F., and Luo, Y. (2006). Direct quantification of gene expression in homogenates of formalin-fixed, paraffin-embedded tissues. Biotechniques *40*, 481–486.

Yang, Y., Fricke, T., and Diaz-Griffero, F. (2013). Inhibition of reverse transcriptase activity increases stability of the HIV-1 core. J. Virol. *87*, 683–687.

Zhang, R., Mehla, R., and Chauhan, A. (2010). Perturbation of host nuclear membrane component RanBP2 impairs the nuclear import of human immunodeficiency virus -1 preintegration complex (DNA). PLoS ONE *5*, e15620.

Zhu, J., Davoli, T., Perriera, J.M., Chin, C.R., Gaiha, G.D., John, S.P., Sigiollot, F.D., Gao, G., Xu, Q., Qu, H., et al. (2014). Comprehensive identification of host modulators of HIV-1 replication using multiple orthologous RNAi reagents. Cell Rep. *9*, 752–766.